http://dx.doi.org/10.5012/bkcs.2012.33.1.183

Synthesis and Crystal Structure of Blue Phosphorescent *mer*-Tris(2',6'-difluoro-2,3'-bipyridinato-*N*,$C^{4'}$) Iridium(III)

Narae Jung, Eunji Lee, Jinho Kim, Hyoungkeun Park, Ki-Min Park,†,* and Youngjin Kang*

Division of Science Education & Department of Chemistry, Kangwon National University, Chuncheon 200-701, Korea
**E-mail: kangy@kangwon.ac.kr*
†Department of Chemistry and Research Institute of Natural Science, Gyeongsang National University, Jinju 660-701, Korea
**E-mail: kmpark@gnu.ac.kr*
Received November 10, 2011, Accepted November 18, 2011

A blue phosphorescent Ir(dfpypy)$_3$ (dfpypy:fluorinated pyridine-pyridine ligand) complex with meridional configuration has been synthesized by newly developed effective method and its solid state structure and photoluminescence are characterized. For this complex, *mer*-Ir(dfpypy)$_3$, the glass-transition and decomposition temperatures appear at 160 ºC and 384 ºC respectively in TGA and DSC experiments, which indicates that this complex has high thermal stability. In a crystalline structure, an average Ir-C bond length of *mer*-Ir(dfpypy)$_3$ is slightly longer than that of *fac*-Ir(dfpypy)$_3$, which assumed to be due to the weak trans-influence. The absorption and emission spectra are observed more red-shifted in *mer*-Ir(dfpypy)$_3$ than *fac*-Ir(dfpypy)$_3$. In addition, the former is readily oxidized than the latter in electrochemical behavior.

Key Words : Blue phosphorescence, Facial/meridional isomer, Thermal property, Crystal structure, Photophysical property

Introduction

Ir(III) complexes with C^N chelated ligand such as phenylpyridine(ppy) have attracted much attention because of their applicability to Phosphorescence Organic Light-Emitting Diodes (PHOLEDs).[1] In general, homoleptic tris-Ir(III) complexes with this asymmetric chelated ligand (C^N) have two isomers; facial and meridional configurations.[2] There are a number of reports regarding effective synthetic method, photophysical and electrochemical behaviors of Ir(III)(C^N)$_3$ derivatives with facial configuration due to their long-term stability in device operation.[3] In the mean time, the effective synthesis of deep blue phosphorescent Ir(III) complexes become a major issue in the research field mainly because of two reasons; one, the number of phosphorescent complexes applicable to OLEDs is very limited compared to that of green and red complexes, and the other, blue phosphorescent complexes generally diminish the lifetime of devices.[4]

To date, efforts on finding effective synthetic method of deep blue phosphorescent materials have been continued with variation of reaction conditions.[5] Development of deep blue phosphorescent materials is continuously attempted by variations of substituents together with explorations of optimum conditions. For example, in order to obtain deeper HOMO energy, electron-withdrawing substituents such as fluorine has been introduced into the phenyl ring of ppy ligand.[6] Introduction of fluorinated substituent onto the ppy results in the diminution of concentration quenching luminescence and high volatility of ppy based Ir(IIII) complexes as well,[7] which especially makes them deposit readily on the layer under vacuum. Recently, an effective synthetic method of blue *fac*-Ir(III) complexes using Ag(I) and fluorinated ppy ligand has been published by Grushin.[7]

We were able to synthesize a novel *fac*-Ir(III) complex using a fluorinated pyridine-pyridine (**dfpypy**) ligand[4a] during our efforts for developing luminescent materials.[8] This complex was synthesized by the reaction of Ir(acac)$_3$ and **dfpypy** in glycerol at high temperature (reflux condition). However, this reaction requires high cost and much efforts to isolate Ir(**dfpypy**)$_3$ complex. In addition, a pure *fac*-Ir(**dfpypy**)$_3$ has been obtained in a poor yield (> 20%) under the condition. Therefore, we have attempted synthesis of Ir(**dfpypy**)$_3$ using silvertrifluoroacetate under different reaction condition, envisioning that *fac*-Ir(**dfpypy**)$_3$ could be obtained as a major component. Contrary to our expectation, however, *fac*-Ir(**dfpypy**)$_3$ was isolated in a poor yield, while *mer*-Ir(**dfpypy**)$_3$ was obtained in more than 40% yield. Although *mer*-Ir(III) derivatives have shown unique photo/electrochemical nature, they have attracted little attention compared to *fac*-Ir(III) derivatives. Moreover, reports for the synthetic details and the derivatization of *mer*-Ir(III) complexes are very scarce relative to those of *fac*-Ir(III) complexes. These facts prompted us to systematically investigate synthetic methodology and photophysical properties of *mer*-Ir(III) complexes. Herein, we report synthetic details, crystal structure and photophysical property of blue phosphorescent *mer*-Ir(**dfpypy**)$_3$.

Results and Discussion

Complex *mer*-Ir(**dfpypy**)$_3$ was synthesized by a slight modification of a previous synthetic methodology.[7] By the reaction of $IrCl_3$ with 10 equivalents of ligand in the pre-

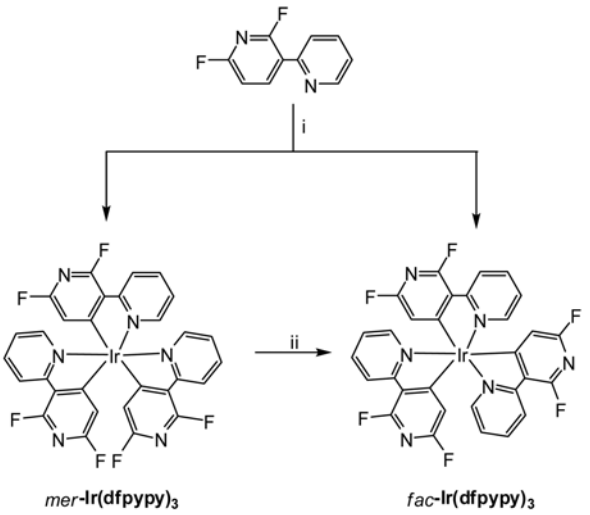

Scheme 1. *Reagent & condition*: i) $IrCl_3 \cdot xH_2O$, $Ag(CF_3COO)$, 180 °C, 4 hr ii) glycerol, reflux (210 °C), 12 h; UV (λ = 254 nm), 12 h, CH_2Cl_2.

sence of $AgCF_3COO$ at 180 °C, complex *mer*-Ir(**dfpypy**)$_3$ was obtained in a moderate yield (40%), as shown in Scheme 1. The formation of *fac*-Ir(**dfpypy**)$_3$ as a minor component was also observed under this reaction condition. Even though reaction temperature is raised up to 200, *mer*-Ir(**dfpypy**)$_3$ was also obtained as a major product. According to previous reports, C^N chelated *fac*-Ir(III) complex was mainly formed at > 200 °C, while *mer*-Ir(III) was formed at < 200 °C.[2] However, when Ag(I) is used as a chlorine scavenger, *mer*-Ir(III) was highly yielded at even high temperature (> 200 °C). We carried out additional experiment in order to convert *mer*-Ir(**dfpypy**)$_3$ into *fac*-Ir(**dfpypy**)$_3$. A *mer*-Ir(**dfpypy**)$_3$ was converted into *fac*-Ir(**dfpypy**)$_3$ under either of the two conditions: A *mer*-Ir(dfpypy)$_3$ in CH_2Cl_2 was irradiated UV light (λ = 254 nm) and a *mer*-Ir(dfpypy)$_3$ in glycerol was heated to 210 °C. However, *fac*-Ir(**dfpypy**)$_3$ was isolated in poor yields (< 10%) under both reaction conditions.

The structure of *mer*-Ir(**dfpypy**)$_3$ was established by using varied spectroscopic methods. In particular, ^{1}H-NMR spectroscopy is one of powerful tools in structural determination of *fac*/*mer*-Ir(III) complexes. Because three **dfpypy** ligands bounded to Ir metal center (an inherent C_1 symmetry) with meridional configuration are magnetically inequivalent. As expected, more complicated resonances and equal numbers between the resonances and the protons in aromatic region are observed in ^{1}H-NMR, as shown in Figure 1. Moreover, six well resolved doublet peaks appeared in ^{19}F-NMR; The peak at δ −71.1 ppm is due to the overlap of two doublet peaks. Both NMR results are direct evidences that synthesized complex has meridional configuration.

To investigate the thermal stability of *mer*-Ir(**dfpypy**)$_3$, thermogravimetric analysis (TGA) and differential scanning calorimetry (DSC) was conducted. If a molecule is suitable for use in OLEDs, it should have high decomposition (T_d) and glass transition (T_g) temperature. T_d value of more than

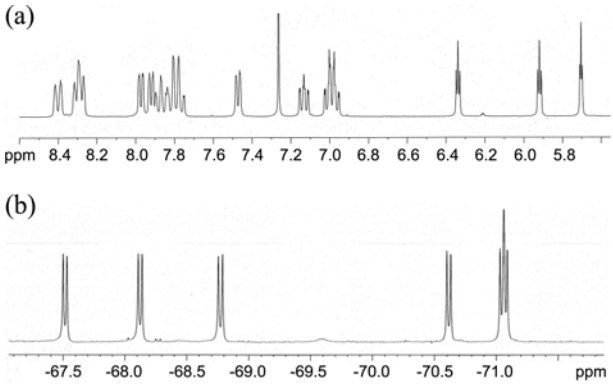

Figure 1. ^{1}H-NMR (a) and ^{19}F-NMR (b) spectra of *mer*-**Ir(dfpypy)$_3$**.

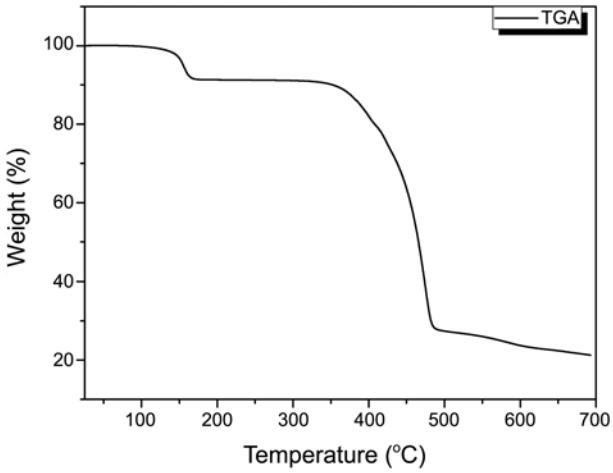

Figure 2. TGA curve of *mer*-**Ir(dfpypy)$_3$** under N_2 atmosphere.

300 °C should be high enough to deposit molecules without any decomposition under reduced pressure. To guarantee morphological stability of molecules, T_g value should exceed 110 °C, because joule heat occurs inevitably during the operation of the device.[9] As shown in Figure 2, the TGA curve of *mer*-Ir(**dfpypy**)$_3$ exhibits thermal stability up to 320 °C. The weight loss of *ca.* 10% appears at around 150 °C which could be originated from solvent molecule of crystal lattice (see description of crystal structure). Subsequently, no loss of weight was observed up to 320 °C while the decomposition temperature which is defined as a 5% loss of weight appeared at 384 °C. This result indicates that complex *mer*-Ir(**dfpypy**)$_3$ is less stable than *fac*-[Ir(ppy)$_3$](423 °C) and *fac*-[Ir(**dfpypy**)$_3$](452 °C).[4a] However, T_g was observed at 159.8 °C, followed by melting at 383 °C in DSC experiment (see supporting information).

The structure of *mer*-Ir(**dfpypy**)$_3$ was clearly established by single-crystal X-ray diffraction analysis. The crystal structure and packing diagram of *mer*-Ir(**dfpypy**)$_3$ are presented in Figure 3 and Figure 4, respectively. The general features of the complex *mer*-Ir(**dfpypy**)$_3$ are similar to those of our recent related structure with facial configuration with distorted octahedral geometry around the Ir center.[4a] The Ir center in complex *mer*-Ir(**dfpypy**)$_3$ is six-coordinated by three C atoms and three N atoms from three chelating

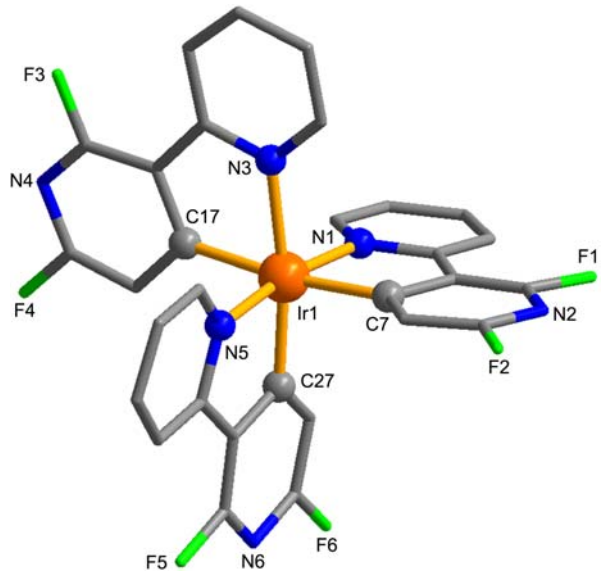

Figure 3. Coordination environment of the Ir(III) ion in complex **1** with selected numbering scheme. All hydrogen atoms and solvent molecules are omitted for clarity. Selected bond lengths (Å) and angles (deg): Ir1-N1 2.064(7), Ir1-N3 2.137(7), Ir1-N5 2.049(7), Ir1-C7 2.047(9), Ir1-C17 2.031(9), Ir1-C27 1.994(9), N1-Ir1-N3 91.8(3), N1-Ir1-N5 170.9(3), N1-Ir1-C7 79.5(3), N1-Ir1-C17 96.8(3), N1-Ir1-C27 93.1(3), N3-Ir1-N5 95.3(3), N3-Ir1-C7 95.9(3), N3-Ir1-C17 77.7(3), N3-Ir1-C27 171.4(3), N5-Ir1-C7 94.1(3), N5-Ir1-C17 90.3(3), N5-Ir1-C27 80.5(3), C7-Ir1-C17 172.6(4), C7-Ir1-C27 92.0(4), C17-Ir1-C27 94.7(4).

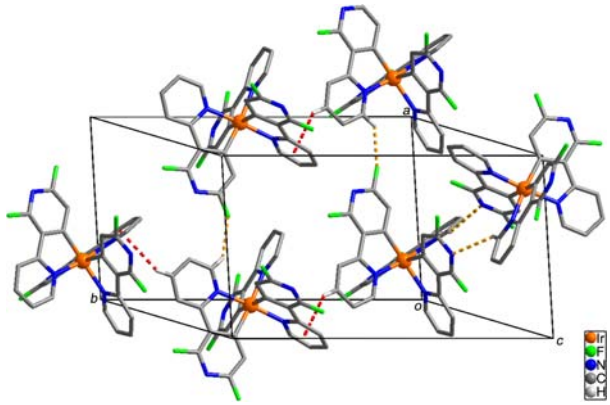

Figure 4. Crystal packing structure of **1**. Dotted lines represent intermolecular interactions: The C-H···X (X = N or F) hydrogen bonds, brown; edge-to-face C-H···π, red. Solvent molecules and H atoms not involved in intermolecular interactions have been omitted for clarity.

dfpypy ligands, forming a distorted octahedral geometry due to narrow ligand bite angles ranging from 77.7(3) to 96.8(3)°. The Ir-C bond lengths (average: 2.026(9) Å) observed in *mer*-Ir(**dfpypy**)$_3$ are slightly longer than those of the *fac*-Ir(dfpypy)$_3$ complex (Ir-C(*av*) = 2.001(5) Å).[4a] However, the Ir-N bond length, ranging from 2.049(7) to 2.137(7) Å, is slightly shorter than those of *fac*-Ir(**dfpypy**)$_3$ (2.116(4)-2.135(4) Å). These results can be due to weak trans-influence in *mer*-Ir(**dfpypy**)$_3$. Within the ligands, the two pyridine rings are approximately coplanar with the maximum dihedral angle rings being 7.7(6)°.

Table 1. Structural Parameters of Hydrogen Bonds and Intermolecular Interactions for *mer*-**Ir(dfpypy)$_3$** (Å and deg)[a]

D-H···A	d(D-H)	d(H···A)	d(D···A)	< (DHA)
C1-H1···N2[b]	0.93	2.66	3.325(14)	129.3
C11-H11···N4[c]	0.93	2.69	3.301(14)	123.6
C21-H21···F6[d]	0.93	2.34	3.074(12)	135.4
C-H···π interaction				
C23-H23···Cg1[e]	0.93	2.95	3.76	146.2

[a]Cg1 defines the centroid of pyridyl ring including N1. Symmetry codes given in foodnotes *b*–*e*. [b]$x + 0.5, -y + 0.5, z + 0.5$, [c]$x - 0.5, -y + 0.5, z - 0.5$, [d]$x - 1, y, z$, [e]$-x + 0.5, y + 0.5, -z + 1.5$.

In the crystal packing structure of *mer*-Ir(**dfpypy**)$_3$, as shown in Figure 4, weak intermolecular hydrogen bonds such as the C-H···N and C-H···F type are observed. The distances of H···N and H···F are in the range of 2.34-2.69 Å (Table 1). In addition, weak intermolecular edge-to-face C-H···π(py) interaction also exists in the crystal packing structure. These intermolecular interactions contribute to the stabilization of the crystal packing, in agreement with the result of TG analysis. The structural parameters for the intermolecular interactions are summarized in Table 2. In the unit cell, the solvent molecules such as dichloromethane with the site occupancy of 0.5 only occupied the void between complexes. There is no evidence of intermolecular interactions between solvent molecules and complex.

UV/vis and photoluminescent spectra were measured in a dilute CH_2Cl_2 solution, as shown in Figure 5. As expected, when being irradiated by UV light, complex *mer*-Ir(**dfpypy**)$_3$ showed a bright blue emission. A single intense absorption band which is attributed to the $^1\pi$-π^* transition is observed at 250 nm, whereas *fac*-Ir(**dfpypy**)$_3$ exhibits two intense absorption bands at 240 nm and 260 nm respectively. In addition, less intense singlet metal-to-ligand charge transfer (^{1}MLCT) band with smaller extinction (ε = 5500, M^{-1} cm^{-1}) than in *fac*-Ir(**dfpypy**)$_3$ is observed at 360 nm. The red-shifted absorption band in mer-Ir(III) complexes is typical. The same observation are reported in Ir(C^N)$_3$

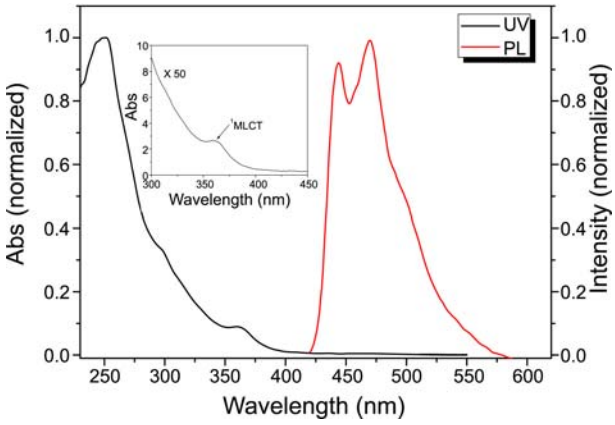

Figure 5. Absorption and emission spectra of *mer*-**Ir(dfpypy)$_3$** in CH_2Cl_2 at room temperature.

analogues such as *fac*/*mer*-Ir(tpy)$_3$ and *fac*/*mer*-Ir(dfppy)$_3$.[2]

There is a striking difference between *mer*-Ir(**dfpypy**)$_3$ and other *mer*-Ir(C^N)$_3$ analogues in emission behavior. According to previous reports, most of *mer*-Ir(C^N)$_3$ showed very broad and non-resolved emission bands.[2,10] This result indicates that the geometry of excited state is further distorted form than that of the ground state. For this complex, a broad emission bands with the same full-width at half maximum (fwhm: 65 nm) compared to *fac*-Ir(**dfpypy**)$_3$ is observed, as shown in Figure 5. In general, the emission band from MLCT states are broad and featureless, while the highly structured emission band is mainly originated from the $^3\pi$-π^* state.[11] Accordingly, the emission observed in *mer*-Ir(**dfpypy**)$_3$ is attributable to the $^3\pi$-π^* with the contribution of MLCT transition. A little difference between *fac*-Ir(**dfpypy**)$_3$ and *mer*-Ir(**dfpypy**)$_3$ exists in emission spectrum. Both complexes showed two intense emission maximum in CH_2Cl_2 at room temperature. The intensity of two maximum peaks is almost the same in *fac*-Ir(**dfpypy**)$_3$, while the intensity of longer wavelength (470 nm) is higher than the other maximum peak (443 nm) in *mer*-Ir(**dfpypy**)$_3$.

Assuming that the photoluminescence (PL) quantum yield (Φ_{PL}) of *fac*-Ir(**dfpypy**)$_3$ is 100%, the Φ_{PL} of *mer*-Ir(**dfpypy**)$_3$ was determined to be 30% (± 10%) in degassed CH_2Cl_2 solution at room temperature. The bond dissociation in the excited state is regarded as one of emission quenching process. Therefore, the diminution of Φ_{PL} could be due to the weak Ir-C bond of *mer*-Ir(**dfpypy**)$_3$ in the excited state, as supported by the crystal structure.

The electrochemical property of *mer*-Ir(**dfpypy**)$_3$ were characterized using cyclic voltammetry (CV) versus Ag/AgCl with a ferrocene/ferrocenium (Fc/Fc^+) internal standard.

The quasi-reversible oxidation is observed at 1.36 V (E_{pa}), as shown in Figure 6. It is noteworthy that the complex shows lower oxidation potentials than that of *fac*-Ir(**dfpypy**)$_3$ (E_{pa} = 1.78 V), indicating that a relative ease of oxidation exist.

The onset potentials of oxidation appeared at 1.34 V, (*vs* Ag/AgCl), corresponding to 1.17 V (*vs* Fc/Fc^+). Based on these observations, the HOMO levels were estimated using an oxidation potential of ferrocene/ferrocenium (4.8 eV below the vacuum level).[12] Therefore, the HOMO level is estimated to be −5.97 eV. This value is higher than that of *fac*-Ir(**dfpypy**)$_3$ (−6.20 eV). The LUMO level was estimated from the onset potential of reduction; the estimated values were −3.63 eV, respectively. As expected, there is a little difference between the *meridional* and *facial* isomers in electrochemical behavior. It can be explained by a lengthening of the transoid Ir-C bonds in the *mer*-isomer. Consequently, it brings about stabilizing the HOMO to a significant extent, while slightly stabilizing the LUMO.[2]

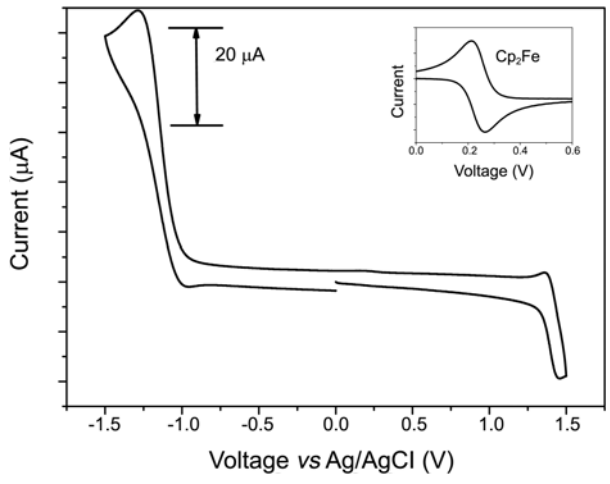

Figure 6. Cyclic voltammogram of *mer*-**Ir(dfpypy)**$_3$ measured in CH_3CN/CH_2Cl_2 using Ag/AgCl (0.5 mM) as a reference electrode and Bu_4NPF_6 as an electrolyte at a scan rate of 100 mV/s.

Experimental Methods

General Considerations. All experiments were performed under a dry N_2 atmosphere using standard Schlenk techniques. All solvents were freshly distilled over appropriate drying reagents prior to use. All starting materials were purchased from either Aldrich or Strem and used without further purification.

Measurement. ^{1}H NMR and mass spectra were recorded on a Bruker DRX 400 MHz spectrometer and JEOL-JMS 700 instrument, respectively. UV/vis and photoluminescent spectra for all samples with concentrations in the range of 10-50 μM were obtained from the UV/vis spectrometer Lambda 900 and a Perkin Elmer Luminescence spectrometer LS 50B, respectively. All solutions for photophysical experiments were degassed with more than three repeated freeze-pump-thaw cycles in a vacuum line. Cyclic voltammetry was performed with an Autolab potentiostat by Echochemie under a nitrogen atmosphere in a one-compartment electrolysis cell consisting of a platinum wire working electrode, a platinum wire counter electrode, and a quasi Ag/AgCl reference electrode. Cyclic voltammograms were monitored at scan rates of either 100 mVs^{-1} or 50 mVs^{-1} and recorded in distilled dichloromethane/acetonitrile. The concentration of the complex was maintained at 0.5 mM or less and each solution contained 0.1 M of tetrabutylammonium-hexafluorophosphate (TBAP) as the electrolyte. The thermogravimetric spectrum was recorded on a Perkin-Elmer TGA-7 under nitrogen environment at a heating rate of 10 °C/min over a range of 25-700 °C.

X-ray Crystallographic Analysis. Single crystals of *mer*-Ir(**dfpypy**)$_3$ suitable for X-ray analysis were obtained from slow vapor diffusion of hexane into a solution of *mer*-Ir(**dfpypy**)$_3$ in dichloromethane. Single crystal diffraction data of *mer*-Ir(**dfpypy**)$_3$ were collected on a Bruker Smart diffractometer equipped with a graphite monochromated Mo $K\alpha$ (λ = 0.71073 Å) radiation source, operating at 50 kV and 30 mA with a CCD detector. The 45 frames of two dimensional diffraction images were collected at room temperature and processed to obtain the cell parameters and orientation matrix. A total of 1271 frames of two-dimensional diffraction images were collected, each of which was measured for 5 sec. Decay was monitored by 50 standard data frames

Table 2. Crystal Data and Structure Refinement for *mer*-**Ir(dfpypy)$_3$**

empirical formula	$[IrC_{30}H_{15}N_6F_6](CH_2Cl_2)$
formula weight	850.61
crystal system	monoclinic
space group	$P2_1/n$
a (Å)	10.2076(9)
b (Å)	19.6690(17)
c (Å)	17.2640(15)
β (deg)	104.857(2)
V (Å^3)	3350.3(5)
Z	4
D(calcd) (g cm^{-1})	1.686
μ (mm^{-1})	4.209
F(000)	1640
scan type	j-w
no. of reflections collected	18610
no. of independent reflections	6544
absorption correction	Semi-empirical from equivalents
goodness of fit	1.012
R_1, wR_2 [$I > 2s(I)$]	0.0577, 0.1419
R_1, wR_2 (all data)	0.0740, 0.1499

measured at the beginning and end of data collection. No significant decay was observed during the data collection. The frame data were processed to give structure factors using the SAINT-plus.[13] Semi-empirical absorption corrections were applied to the data sets using the SADABS.[13] The structure was solved by direct methods and refined by full matrix least squares methods on F^2 for all data using SHELXTL software.[14] All non-hydrogen atoms of *mer*-Ir(**dfpypy**)$_3$ were refined anisotropically. The hydrogen atoms were placed in calculated positions and refined using a riding model with isotropic thermal parameters 1.2 times those of the parent atoms.

Complex *mer*-Ir(**dfpypy**)$_3$ crystallizes with two crystallographically independent molecules of dichloromethane. The solvent molecules are disordered with occupancies of 0.5 obtained the refinement of the site occupancy factor. All thermal parameters of the solvent molecules were refined using ISOR and DFIX commands because their thermal parameters became unreasonably large or small. Crystallographic data and structural refinement data for *mer*-Ir(**dfpypy**)$_3$ are summarized in Table 2. Selected bond lengths and angles for *mer*-Ir(**dfpypy**)$_3$ are given in Figure 3. The refined atomic coordinates and anisotropic thermal parameters are deposited in the Supporting Information. Crystallographic data (cif files for *mer*-Ir(**dfpypy**)$_3$) for the structure reported here have been deposited with the Cambridge Crystallographic Data Center (Deposition No. CCDC-838888. The data can be obtained free of charge via http://www.ccdc.cam.ac.uk/perl/catreq/catreq.cgi (or from the CCDC, 12 Union Road, Cambridge CB2 1EZ, UK; fax, +44 1223 336033; e-mail, deposit@ccdc.cam.ac.uk).

Synthesis of *mer*-Ir(dfpypy)$_3$. Ligand dfpypy (1 g, 5.20 mmol), $IrCl_3 \cdot xH_2O$ (0.18 g, 0.52 mmol) and silver trifluoro acetate (0.46 g, 2.08 mmol) were charge into a 50 mL round-bottom flask. The mixture was stirred and heated to 180 °C under nitrogen for 4 h. The reaction mixture was then cooled to room temperature, and extracted with CH_2Cl_2 (100 mL). The CH_2Cl_2 solution containing a crude product was flash chromatographed on a silica column using ethylacetate/dichloromethane (v/v = 3:1, R_f = 0.8) to yield 0.31 g (40%) of material. ^{1}H-NMR ($CDCl_3$, 300 MHz) δ 8.40 (d, J = 8.32 Hz, 1H), 8.29 (t, J = 8.20 Hz, 2H), 7.97 (dd, J = 5.84, 0.90 Hz, 1H), 7.92 (dd, J = 5.60, 0.80 Hz, 1H), 7.82 (m, 3H), 7.47 (dd, J = 6.56, 0.72 Hz, 1H), 7.13 (td, J = 6.56 Hz, 1.16 Hz, 1H), 6.99 (m, 2H), 6.34 (t, J = 2.78 Hz, 1H), 5.92 (t, J = 2.75 Hz, 1H), 5.70 (t, J = 1.93 Hz, 1H); ^{13}C-NMR ($CDCl_3$, 100 MHz) δ 197.7, 195.1, 177.7, 177.6, 164.4, 164.3, 162.9, 162.6, 162.5, 162.3, 162.2, 152.9, 150.9, 147.9, 138.8, 138.3, 137.4, 124.2, 124.0, 123.8, 123.5, 123.3, 123.0, 113.0, 112.7, 109.0, 108.9, 108.7, 107.4, 107.1. (C-F resonance not located); MS (FAB): m/z = 767 [M$^+$] Anal. Calcd for $C_{30}H_{15}F_6N_6Ir$: C, 47.06; H, 1.97; N, 10.98. Found: C, 47.21; H, 1.94; N, 10.87.

Conclusions

In summary, a blue phosphorescent *mer*-Ir(**dfpypy**)$_3$ has been synthesized and characterized in its thermal, photophysical and electrochemical properties, and the nature of its solid-state structure. A *mer*-Ir(**dfpypy**)$_3$ has been synthesized in the presence of Ag(I) at 180 °C in a moderate yield. A meridional isomer can be converted to the facial form either at high temperature or at UV light. The meridional configuration can give rise to several distinct characteristics, impacting its solid-state structure, the electrochemical behavior and photoluminescence. In crystal structure, a weak trans-influence is observed. The absorption and emission bands closely resemble in both isomers, while MLCT and emission bands in meridional isomer are more red-shifted. The meridional isomer was oxidized readily relative to the facial isomer. Further study on OLEDs performance using this complex is being investigated in our laboratory.

Acknowledgments. This research was supported by Basic Science Research Program through the National Research Foundation of Korea (NRF) funded by the Ministry of Education, Science and Technology (2011-0010518). Moreover, this work was supported by the industrial strategic technology development program (10039141) funded by the Ministry of Knowledge Economy (MKE, Korea).

References

1. Chi, Y.; Chou, P.-T. *Chem. Soc. Rev.* **2010**, *39*, 638-655 references cited therein.
2. Tamayo, A. B.; Alleyne, B. D.; Djurovich, P. I.; Lamansky, S.; Tsyba, I.; Ho, N. N.; Bau, R.; Thompson, M. E. *J. Am. Chem. Soc.* **2003**, *125*, 7377-7387.
3. Chew, S.; Lee, C. S.; Lee, S.-T.; Wang, P.; He, J.; Li, W.; Pan, J.; Zhang, X.; Kwong, H. *Appl. Phys. Lett.* **2006**, *88*, 093510-093510-3.

4. (a) Lee, J.; Park, K.-M.; Yang, K.; Kang, Y. *Inorg. Chem.* **2009**, *48*, 1030-1037. (b) Sajoto, T.; Djurovich, P. I.; Tamayo, A.; Yousufuddin, M.; Bau, R.; Thompson, M. E.; Holmes, R. J.; Forrest, S. R. *Inorg. Chem*. **2005**, *44*, 7992-8003. (c) Yeh, Y.-S.; Cheng, Y.-M.; Chou, P.-T.; Lee, G.-H.; Yang, C.-H.; Chi, Y.; Shu, C.-F.; Wang, C.-H. *ChemPhysChem.* **2006**, *7*, 2294-2297 references cited therein.
5. Ren, X.; Li, J.; Holmes, R. J.; Djurovich, P. I.; Forrest, S. R.; Thompson, M. E. *Chem. Mater*. **2004**, *16*, 4743-4747.
6. Lamansky, S.; Djurovich, P.; Murphy, D.; Abdel-Razzaq, F.; Kwong, R.; Tsyba, I.; Bortz, M.; Mui, B.; Bau, R.; Thompson, M. E. *Inorg. Chem*. **2001**, *40*, 1704-1711.
7. Grushin, V. V.; Herron, N.; LeCloux, D. D.; Marshall, W. J.; Petrov, V. A.; Wang, Y. *Chem. Commun*. **2001**, 1494-1495.
8. (a) Ji, H.; Kim, J.; Yoo, J. W.; Lee, H. S.; Park, K.-M.; Kang, Y. *Bull. Korean Chem. Soc*. **2010**, *31*, 1371-1374. (b) Lee, E.; Jung, N.; Kim, H.; Park, K.-M.; Kim, J.; Kang, Y. *Bull. Korean Chem. Soc*. **2010**, *31*, 3021-3024. (c) Ko, S.; Choi, H.; Kang, M.-S.; Hwang, H.; Ji, H.; Kim, J.; Ko, J.; Kang, Y. *J. Mater. Chem*. **2010**, *20*, 2391-2399. (d) Jung, H.; Hwang, H.; Park, K.-M.; Kim, J.; Kim, D.-H.; Kang, Y. *Organometallics* **2010**, *29*, 2715-2723.
9. Rothmann, M. M.; Fuchs, E.; Schildknecht, C.; Langer, N.; Lennartz, C.; Munster, I.; Strohriegl, P. *Org. Electron*. **2011**, *12*, 1192-1197.
10. Ide, N.; Matsusue, N.; Kobayashi, T.; Naito. H. *Thin Solid Films* **2006**, *509*, 164-167.
11. Hong, H.-W.; Chen, T.-M. *Mater. Chem. Phys.* **2007**, *101*, 170-176.
12. Lee, S. H.; Jang, B.-B.; Tsutsui, T. *Macromolecules* **2002**, *35*, 1356-1364.
13. Bruker, SMART and SAINT: *Area Detector Control and Integration Software Ver. 5.0*; Bruker Analytical X-ray Instruments: Madison, Wisconsin, 1998.
14. Bruker, SHELXTL: *Structure Determination Programs Ver. 5.16*; Bruker Analytical X-ray Instruments: Madison, Wisconsin, 1998.